Dynamic Multi-Domain Bipedal Walking with ATRIAS through SLIP based Human-Inspired Control*

Ayonga Hereid
AMBER Lab
Texas A&M University
College Station, TX 77843
ayonga@tamu.edu

Shishir Kolathaya
AMBER Lab
Texas A&M University
College Station, TX 77843
shishirny@tamu.edu

Mikhail S. Jones
Dynamic Robotics Laboratory
Oregon State University
Corvallis, OR 97331
jonesmik@engr.orst.edu

Johnathan Van Why
Dynamic Robotics Laboratory
Oregon State University
Corvallis, OR 97331
vanwhyj@onid.orst.edu

Jonathan W. Hurst
Dynamic Robotics Laboratory
Oregon State University
Corvallis, OR 97331
jonathan.hurst@oregonstate.edu

Aaron D. Ames
AMBER Lab
Texas A&M University
College Station, TX 77843
aames@tamu.edu

ABSTRACT

This paper presents a methodology for achieving efficient multi-domain underactuated bipedal walking on compliant robots by formally emulating gaits produced by the Spring Loaded Inverted Pendulum (SLIP). With the goal of achieving locomotion that displays phases of double and single support, a hybrid system model is formulated that faithfully represents the full-order dynamics of a compliant walking robot. The SLIP model is used as a basis for constructing human-inspired controllers that yield a dimension reduction through the use of hybrid zero dynamics. This allows for the formulation of an optimization problem that produces hybrid zero dynamics that best represents a SLIP model walking gait, while simultaneously ensuring the proper reduction in dimensionality that can be utilized to produce stable periodic orbits, i.e., walking gaits. The end result is stable robotic walking in simulation and, when implemented on the compliant robot ATRIAS, experimentally realized dynamic multi-domain locomotion.

Categories and Subject Descriptors

J.2 [**Physical Sciences and Engineering**]: [engineering, mathematics and statistics; G.1.6 [**Numerical Analysis**]: Optimization - constrained optimization

Keywords

SLIP model, multi-domain hybrid systems, bipedal walking, hybrid zero dynamics, human-inspired optimization

*This research is supported by CPS grant 1239085 and SRI grant W31P4Q-13-C-009.

HSCC'14, April 15–17, 2014, Berlin, Germany.

http://dx.doi.org/10.1145/2562059.2562143.

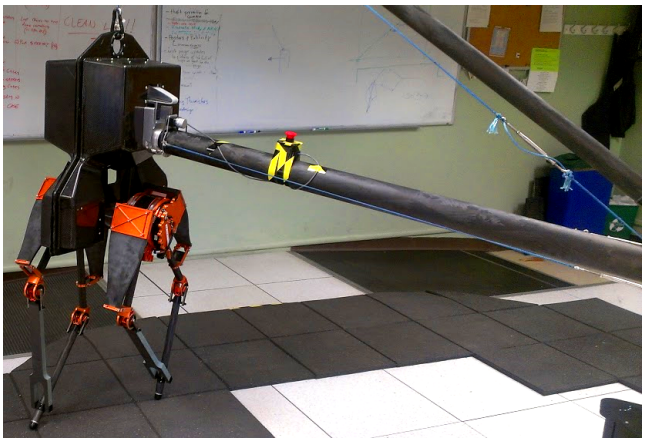

Figure 1: Figure showing front view of ATRIAS. Its motion is constrained to the sagittal plane through a boom connected to its torso.

1. INTRODUCTION

Humans are able to walk with exceptional ease and efficiency. It is postulated that this is due to two major factors: the presence of elasticity in their joints [20], and a mass distribution aimed at conservation of energy [16]. In the case of the former, elasticity allows energy that would otherwise be lost to be stored and used later to replace actuator work. For example, humans handle impacts during a foot strike by storing the kinetic energy rather than dissipating it, then converting the stored energy back to kinetic energy before the end of the step. In fact, [11] shows that the efficiency increases steadily when the positive work is mainly derived from the passive recoil of muscle elastic elements and to a lesser extent from the active shortening of the contractile machinery. In the latter, the mass distribution of humans allows them to be likened to an inverted pendulum model which can swing forward with constant energy; human walking is therefore analogous to the motion of coupled pendula, where the stance leg behaves like an inverted pendulum moving about the stance foot, and the swing leg like a regular

pendulum swinging about the hip. This points to reduced models of human locomotion centered around inverted compliant pendula.

Reduced order dynamic models have long been used in biomechanics and robotics to encapsulate the most important dynamic properties of complex systems [12, 17, 21]. The Spring Loaded Inverted Pendulum (SLIP), based upon the concept of coupled compliant pendula, is one such low-dimensional model that has been shown to approximate animal walking and running behaviors in everything from cockroaches, to quail, to kangaroos [9], to humans [8]. ATRIAS, shown in Fig. 1, is a 5-DOF under-actuated robot with series compliance specifically constructed so as to capture the essential elements of the SLIP model and thereby allow for the realization of efficient and natural locomotion on bipedal robots.

The goal of this paper is to provide a formal framework in which to realize SLIP inspired walking gaits on bipedal robots, and realize these formally-generated gaits experimentally to achieve natural locomotion. With this goal in mind, we begin by considering a hybrid system model of ATRIAS. Since it has been shown that humans display multiple discrete phases of walking consisting of double and single support [10, 6], we construct a multi-domain hybrid system model capturing these different phases of walking. In order to achieve the dimensionality reduction enjoyed by the SLIP model, we utilize human-inspired control [4, 3] to construct virtual constraints that project the full-order dynamics of the system to a reduced order model expressed via multi-domain hybrid zero dynamics [18, 22, 23]. A formal result establishes that stable periodic orbits, i.e., walking gaits, for the reduced dynamics imply stable periodic orbits for the full-order dynamics. This observation is utilized in the construction of a SLIP inspired optimization; in particular, walking gaits generated for the SLIP model are used as the cost in an optimization aimed at achieving hybrid invariance of the reduced order dynamics. Novel constructions are utilized to both make this problem computationally tractable and to allow for the inclusion of constraints that will ensure the physical realizability of the resulting walking gaits.

The SLIP-inspired methodology for generating dynamic multi-domain gaits on compliant bipedal robots is applied to ATRIAS both in simulation and experiment. The behavior of the gait is compared against the SLIP walking gait from which it was obtained, and the methods for translating the theoretic constructions to hardware are outlined. The end result is the experimental implementation on ATRIAS and successful demonstration of dynamic multi-domain locomotion. Moreover, the locomotion is remarkably natural looking.

2. MULTI-DOMAIN HYBRID SYSTEM

This section describes the hybrid model of the bipedal robot ATRIAS in detail. ATRIAS (**A**ssume **T**he **R**obot **I**s **A** **S**phere) is a 3D capable, human-scale, bipedal robot conceived and implemented at the Oregon State University Dynamic Robotics Laboratory. Designed to match key characteristics of the SLIP model, ATRIAS uses large springs in series with actuators to drive lightweight four bar mechanisms on each leg which terminate in point feet. This enables ATRIAS to achieve agile, efficient and highly dynamic maneuvers. For the current work, a support boom is used

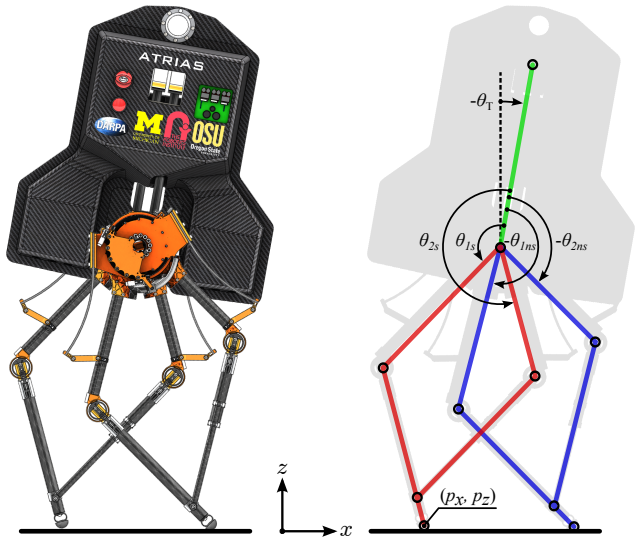

Figure 2: The coordinate configuration of the robot.

to constrain torso rotation and translation to the sagittal plane, effectively planarizing the dynamics. A more detailed description of the robot is presented in [14]. Fig. 1 illustrates the experimental setup.

Robot Configuration. For the 2D model of ATRIAS, we will consider the generalized coordinates of the robot due to the multi-domain structure of the hybrid system. That is, the stance toe position $\{p_x, p_z\}$ and torso pitch angle θ_T of the body fixed frame with respect to world inertia frame will be introduced as the extended coordinates of the robot. By the nature of the parallelogram of four link bars, only two coordinates are needed to characterize each leg, as shown in Fig. 2, where $\{\theta_{1s}, \theta_{2s}\}$ are the angles of the upper two bars of stance leg, $\{\theta_{1ns}, \theta_{2ns}\}$ are the angles of upper two bars of the non-stance leg with respect to the torso, respectively. Since the motors are connected to legs through springs to introduce compliance, additional coordinates are introduced to model the dynamics of the motors, i.e., $\theta_m = \{\theta_{m1s}, \theta_{m2s}, \theta_{m1ns}, \theta_{m2ns}\}$ are the corresponding angles of motor outputs, measured in the same coordinates of the respective joint angles, where θ_i equals θ_{mi} when there is no spring deflection, with $i \in \{1s, 2s, 1ns, 2ns\}$. Therefore the following configuration space $\mathcal{Q}$ is given in the generalized coordinates:

$$\theta_e = \{p_x, p_z, \theta_T, \theta_b, \theta_m\}^T, \tag{1}$$

where $\theta_b = \{\theta_{1s}, \theta_{2s}, \theta_{1ns}, \theta_{2ns}\}$ are the rigid body coordinates. When there is an impact the legs need to be switched accordingly, which is done by using the reset map.

Hybrid System Model. Having described the basics of the hardware setup, the mathematical model of multi-domain walking for this bipedal robot can thus be designed using the framework of hybrid systems [6]. For this paper, we are concerned with a bipedal walking gait consisting of a *single* and a *double* support phase (see Fig. 3). The formal hybrid model for the two-domain locomotion is given by the *tuple*:

$$\mathscr{HC}_A = (\Gamma_A, \mathcal{D}_A, \mathcal{U}_A, S_A, \Delta_A, FG_A), \tag{2}$$

where

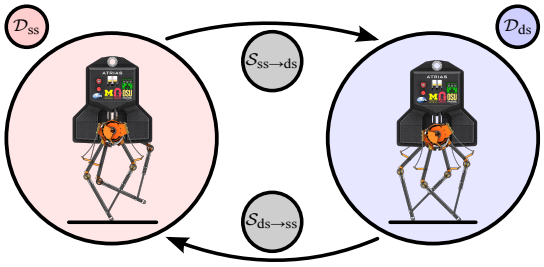

Figure 3: The directed graph of single/double support phase.

- $\Gamma_A = (V_A, E_A)$ is the directed graph specific to this hybrid system, with vertices $V_A = \{\mathbf{ss}, \mathbf{ds}\}$, where **ss** and **ds** represent single and double support phases, respectively, and edges $E_A = \{e_1 = \{\mathbf{ss} \to \mathbf{ds}\}, e_2 = \{\mathbf{ds} \to \mathbf{ss}\}\}$,
- $\mathcal{D}_A = \{\mathcal{D}_{\mathbf{ss}}, \mathcal{D}_{\mathbf{ds}}\}$ is a set of two domains,
- $\mathcal{U}_A = \{\mathcal{U}_{\mathbf{ss}}, \mathcal{U}_{\mathbf{ds}}\}$ is a set of admissible controls,
- $S_A = \{S_{\mathbf{ss}\to\mathbf{ds}}, S_{\mathbf{ds}\to\mathbf{ss}}\}$ is a set of guards,
- $\Delta_A = \{\Delta_{\mathbf{ss}\to\mathbf{ds}}, \Delta_{\mathbf{ds}\to\mathbf{ss}}\}$ is a set of reset maps, and finally
- $FG_A = \{(f_{\mathbf{ss}}, g_{\mathbf{ss}}), (f_{\mathbf{ds}}, g_{\mathbf{ds}})\}$ is a control system on each $\mathcal{D}_v$ for $v \in V_A$.

The two domains $\{\mathcal{D}_{\mathbf{ss}}, \mathcal{D}_{\mathbf{ds}}\}$ are depicted in the Fig. 3. The robot is in the double support phase when both legs are in contact with the ground and transitions to single support phase when one of the legs lifts off the ground. The remainder of this section will be focused on how to construct the individual elements of the two-domain hybrid system considered.

Single Support. In the single support case, the non-stance foot is above the ground. When the non-stance foot strikes the ground, a guard is reached and the transition to the next domain takes place. This implies that the single support domain has the following structure:

$$\mathcal{D}_{\mathbf{ss}} = \{(\theta_e, \dot{\theta}_e, u) : h_{ns}(\theta_e) \geq 0, F^z_{ns}(\theta_e, \dot{\theta}_e, u) = 0\}, \quad (3)$$

where $F^z_{ns}(\theta_e, \dot{\theta}_e, u)$ is the normal force acting on the non-stance foot (as will be formally defined later) and $h_{ns}(\theta_e)$ is the height of the non-stance foot. Similarly, the guard is given by:

$$S_{\mathbf{ss}\to\mathbf{ds}} = \{(\theta_e, \dot{\theta}_e) : h_{ns}(\theta_e) = 0, \dot{h}_{ns}(\theta_e, \dot{\theta}_e) < 0\}. \quad (4)$$

Impacts happens when the non-stance foot hits the ground. The discrete dynamics of the impact of system with compliance can be computed [15, 22] by assuming a perfectly plastic impact of the rigid dynamics and state continuity in the motor positions and velocities [18]; the post-impact states, computed in terms of pre-impact states, is given by:

$$\Delta_{\mathbf{ss}\to\mathbf{ds}}(\theta_e, \dot{\theta}_e) = \begin{bmatrix} \mathcal{R}\Delta_{\theta_e}\theta_e \\ \mathcal{R}\Delta_{\dot{\theta}_e}(\theta_e)\dot{\theta}_e \end{bmatrix}, \quad (5)$$

where $\mathcal{R}$ is the relabeling matrix required to switch the stance and non-stance legs.

The control system $(f_{\mathbf{ss}}, g_{\mathbf{ss}})$ can be obtained from the Lagrangian dynamics of a n-DOF robot. Using the coordinates $\theta = (p_x, p_z, \theta_T, \theta_b)$, we have [18]:

$$D(\theta)\ddot{\theta} + H(\theta, \dot{\theta}) = B_{sp}\tau_{sp}(\theta_b, \theta_m, \dot{\theta}_b, \dot{\theta}_m) + J_s^T(\theta)F_s, \quad (6)$$

$$J_m\ddot{\theta}_m = -\tau_{sp}(\theta_b, \theta_m, \dot{\theta}_b, \dot{\theta}_m) + B_m u, \quad (7)$$

where $D(\theta)$ and $H(\theta, \dot{\theta})$ are obtained from the dynamics of the rigid body system without series compliant actuators, J_m is the motor inertia, $u \in \mathcal{U}$ are the motor control inputs, $B_m \in \mathbb{R}^{4\times4}$ is the motor torques distribution matrix, $J_s(\theta)$ is the Jacobian of the holonomic constraint defined by the height of the stance foot and F_s is the vector of reaction forces acting on the stance foot such that the acceleration of the stance foot is zero and can be computed in terms of state variables and control inputs [13]. Also, $B_{sp} \in \mathbb{R}^{7\times4}$ is the spring force distribution matrix,

$$B_{sp} = \begin{bmatrix} \mathbf{0}_{3\times4} \\ \mathbf{I}_{4\times4} \end{bmatrix}, \quad (8)$$

and $\tau_{sp}(\theta_b, \theta_m, \dot{\theta}_b, \dot{\theta}_m)$ is the vector of spring forces. For series springs, it can be computed by,

$$\tau_{sp}(\theta_b, \theta_m, \dot{\theta}_b, \dot{\theta}_m) = b(\dot{\theta}_m - \dot{\theta}_b) + k(\theta_m - \theta_b), \quad (9)$$

where $k \in \mathbb{R}^{4\times4}$ and $b \in \mathbb{R}^{4\times4}$ are the identified matrices of spring constants and damping coefficients for each spring. Then (6) - (9) can be combined together to give the following control system:

$$\underbrace{\begin{bmatrix} D & \mathbf{0} \\ \mathbf{0} & J_m \end{bmatrix}}_{D_e}\ddot{\theta}_e + \underbrace{\begin{bmatrix} H \\ \mathbf{0} \end{bmatrix}}_{H_e} + \kappa = \underbrace{\begin{bmatrix} \mathbf{0} \\ B_m \end{bmatrix}}_{B_e} u + J_{es}^T F_s, \quad (10)$$

where

$$\kappa = \begin{bmatrix} \mathbf{0}_{3\times4} & \mathbf{0}_{3\times4} \\ k & -k \\ -k & k \end{bmatrix}\begin{bmatrix} \theta_b \\ \theta_m \end{bmatrix} + \begin{bmatrix} \mathbf{0}_{3\times4} & \mathbf{0}_{3\times4} \\ b & -b \\ -b & b \end{bmatrix}\begin{bmatrix} \dot{\theta}_b \\ \dot{\theta}_m \end{bmatrix}, \quad (11)$$

and $J_{es}(\theta_e) = [J_s(\theta) \quad \mathbf{0}]$.

Having obtained the equations of motion, the control system formed by $(f_{\mathbf{ss}}, g_{\mathbf{ss}})$ is given by:

$$f_{\mathbf{ss}} = \begin{bmatrix} \dot{\theta}_e \\ D_e^{-1}(-\kappa - H_e + J_{es}^T F_s) \end{bmatrix}, g_{\mathbf{ss}} = \begin{bmatrix} \mathbf{0} \\ D_e^{-1}B_e \end{bmatrix}. \quad (12)$$

Double Support. In the double support case, the non-stance foot must remain on the ground. Therefore, the double support domain is given by:

$$\mathcal{D}_{\mathbf{ds}} = \{(\theta_e, \dot{\theta}_e, u) : h_{ns}(\theta_e) = 0, F^z_{ns}(\theta_e, \dot{\theta}_e, u) \geq 0\}, \quad (13)$$

where F^z_{ns} is the normal contact force on the nonstance foot. Since the transition from double support to single support occurs when the normal reaction force on the nonstance foot crosses zero, the guard is given by:

$$S_{\mathbf{ds}\to\mathbf{ss}} = \{(\theta_e, \dot{\theta}_e, u) : h_{ns}(\theta_e) = 0, F^z_{ns}(\theta_e, \dot{\theta}_e, u) = 0\}. \quad (14)$$

For the transition from double support to single support, since there are no impacts involved, the states of the robot remain the same. Therefore the reset map from double support to single support is an identity map: $\Delta_{\mathbf{ds}\to\mathbf{ss}} = \mathbf{I}$.

The control system for the double support will be similar to (10) but with an added constraint on the non-stance foot. This constraint will enforce the non-stance foot to remain on the ground. With this equation, (10) can be modified for the double support case in the following manner:

$$D_e\ddot{\theta}_e + H_e + \kappa = B_e u + J_{es}^T(\theta_e)F_s + J_{ens}^T(\theta_e)F_{ns}, \quad (15)$$

where $J_{ens}(\theta_e) = [J_{ns}(\theta) \quad \mathbf{0}]$ with $J_{ns}(\theta)$ is the Jacobian of the x and y position of the non-stance foot. Accordingly, F_{ns} is the vector of reaction forces acting on the non-stance foot such that the acceleration of the non-stance foot is zero. Moreover $F_{ns} = [F_{ns}^x, F_{ns}^z]^T$, where F_{ns}^x is due to the frictional force in the horizontal direction, and F_{ns}^z is the normal force in the vertical direction which is also used in defining $\mathcal{D}_{\mathbf{ss}}, \mathcal{D}_{\mathbf{ds}}$.

Having obtained the equations of motion, the control system formed by $(f_{\mathbf{ds}}, g_{\mathbf{ds}})$ is given by:

$$f_{\mathbf{ds}} = \begin{bmatrix} \dot{\theta}_e \\ D_e^{-1}(-\kappa - H_e + J_{es}^T F_s + J_{ens}^T F_{ns}) \end{bmatrix}, g_{\mathbf{ds}} = g_{\mathbf{ss}}. \quad (16)$$

3. CONTROLLER DESIGN

This section will describe the methods used to determine the required control input to achieve sustainable and robust multi-domain bipedal walking for the given hybrid system. Previous experimental results have yielded single domain locomotion for robots without series elastic actuators [24, 4] through the successful implementation of human-inspired control. A similar approach will be employed here to achieve two-domain walking on ATRIAS. We begin by selecting a walking gait using the ideal SLIP model. Motivated by this gait, human-inspired control is implemented by picking outputs that elucidate the underlying walking structure through the low-dimensional representation, or "virtual model." It is important to note that emulating a SLIP walking gait through the use of outputs will not necessarily result in a viable walking gait due to the hybrid nature of the system; this will be addressed in detail in the following paragraphs. Nevertheless, combining SLIP walking as a guide for gait generation with formal guarantees on the existence of a stable walking gait will ideally result in more human-like locomotion.

SLIP Model. The spring-mass model consists of a point mass m supported by massless spring legs with fixed rest length l_0 and spring constant k. The springs only act on the mass while in contact with the ground and cannot apply forces during swing. For walking, the hybrid dynamic phases are limited to single support and double support. During double support, the system remains entirely passive with takeoff and transition to single support triggered by zero spring force. During single support, the only control input is the swing leg angle α with touchdown and the switch to double support triggered by the swing leg toe touching the ground. Because the dynamics are almost entirely passive and the only control input is the angle of a massless leg, SLIP model gaits require zero net actuator work.

Walking gaits are generated by selecting a fixed swing leg angle that results in an equilibrium gait, that is, a gait where each step's initial conditions match its final conditions. Given a desired average walking speed and a set of model parameters, a non-linear equation solver is used to find all possible equilibrium gaits. Of these gaits, only one will have a symmetric vertical ground force reaction while the others will be asymmetric. We choose to use this single symmetric gait as it has lower peak forces and a more fluid center of mass trajectory as shown in Fig. 4.

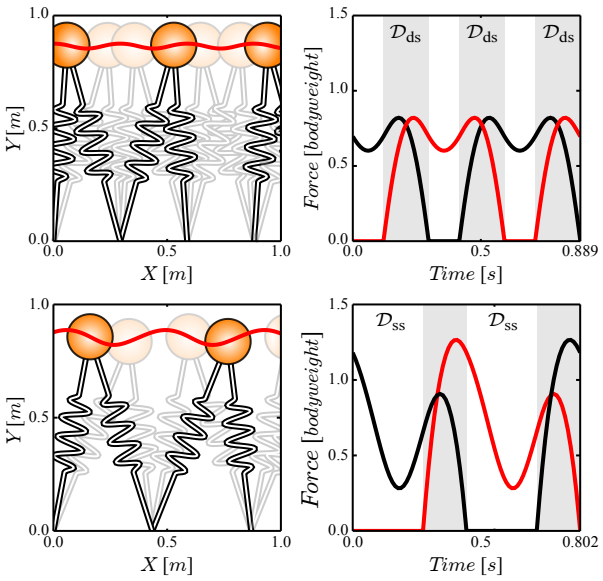

Figure 4: The top plots depict a symmetric SLIP model gait while the bottom plots depict an asymmetric gait. The left plots illustrate the center of mass trajectory and moments of touchdown and takeoff. The plots on the right show the vertical ground reaction force with double support highlighted in grey.

For the purposes of this work we use model parameters that roughly approximate the low-dimensional dynamics of ATRIAS, including the nonlinear spring constant resulting from the four-bar linkage. Doing so enables us to generate relevant center of mass trajectories that take full advantage of the passive dynamics.

Output Definition. As discussed above, the center of mass trajectories are the natural choice to represent the reduced order model. However, for the full-order robotic system, the complex nonlinear expression representing center of mass position will significantly increase the tracking difficulty. Instead, we consider a linear combination of state variables that also capable of approximately characterizing the simple SLIP model dynamics. In particular, the following collection of outputs, first proposed in Eq. (14) of [19], yield such a representation:

- Virtual stance leg angle: $\theta_{sl} := \left(\frac{\theta_{m2s}+\theta_{m1s}}{2}\right)$,
- Virtual non-stance leg angle: $\theta_{nsl} := \left(\frac{\theta_{m2ns}+\theta_{m1ns}}{2}\right)$,
- Stance knee angle: $\theta_{sk} := (\theta_{m2s} - \theta_{m1s})$,
- Non-stance knee angle: $\theta_{nsk} := (\theta_{m2ns} - \theta_{m1ns})$,

where the virtual leg angles characterize the forward motion of the legs and the knee angles determine the corresponding leg lengths. Note that we use motor angles instead of joint angles due to the following considerations: (1) motor angles are directly controlled, therefore we can track them more

precisely, and (2) assuming small spring deflections, motor angles are a good approximation of joint angles which are used to compute center of mass position in the optimization discussed in Sect. 4. The end result is a set of relative degree two outputs for which the corresponding feedback control law is implemented by using input/output linearization.

Canonical Walking Function. The observation that humans and other animals act according to low-dimensional representations during locomotion [2] led to the introduction of the canonical walking function. Defined to be the time solution to a mass-spring-damper system, the canonical walking function is then defined as the linear mass spring damper systems in general mechanical systems:

$$y_H(t,\alpha) = e^{-\alpha_4 t}(\alpha_1 \cos(\alpha_2 t) + \alpha_3 \sin(\alpha_2 t)) + \alpha_5. \quad (17)$$

This becomes apparent by noting that $\alpha_1 = c_0$, $\alpha_2 = \omega_d$, $\alpha_3 = c_1$, $\alpha_4 = \zeta\omega_n$ and $\alpha_5 = g$, where ζ is the damping ratio, ω_n is the natural frequency, $\omega_d = \omega_n\sqrt{1-\zeta^2}$ is the damped natural frequency, c_0 and c_1 are determined by the initial conditions of the system, and g is a gravity related constant.

The canonical walking function is used as the desired trajectories of the previously defined outputs.

Parameterization of Time. *Autonomous* control has several advantages in regard to bipedal robots, the details of which can be found in [7]. Considering this, we introduce a state-based parameterization of time in our system; this is a common practice in [23, 22]. It was observed that the hip position of the SLIP model was monotonously increasing in time. Therefore, the desired outputs's time parameter can be effectively replaced with the robot hip position, yielding the following parameterization of time:

$$\tau(\theta_e) = \frac{\delta p_{\text{hip}}(\theta_e) - \delta p_{\text{hip}}(\theta_e^-)}{\delta p_{\text{hip}}(\theta_e^+) - \delta p_{\text{hip}}(\theta_e^-)}, \quad (18)$$

where $\delta p_{\text{hip}}(\theta_e^-)$ is the forward hip position of the robot at the end of the current step in single support phase, $\delta p_{\text{hip}}(\theta^+)$ is the hip position of the robot at the beginning of the step, with the linearized forward hip position, $\delta p_{\text{hip}}(\theta_e)$, given by:

$$\delta p_{\text{hip}}(\theta_e) = \pi - (L_2 + L_4)\theta_T - L_2\theta_{1s} - L_4\theta_{2s}, \quad (19)$$

where L_2 and L_4 are the lengths of the lower-leg and thigh respectively.

Control Law Construction. Due to the presence of elasticity in ATRIAS, the robot is under-actuated in both *single support* and *double support* phase. Thus we can define the same combination of outputs for both domains. We define the outputs (of relative degree two), as:

$$y(\theta_e) = y^a(\theta_e) - y^d(\tau_i(\theta_e), \alpha), \quad (20)$$

where y^a and y^d are the relative degree two actual outputs and desired outputs, respectively, given by:

$$y^a(\theta_e) = \begin{bmatrix} \theta_{sl}(\theta_e) \\ \theta_{nsl}(\theta_e) \\ \theta_{sk}(\theta_e) \\ \theta_{nsk}(\theta_e) \end{bmatrix}, y^d(\tau,\alpha) = \begin{bmatrix} y_H(\tau,\alpha_{sl}) \\ y_H(\tau,\alpha_{nsl}) \\ y_H(\tau,\alpha_{sk}) \\ y_H(\tau,\alpha_{nsk}) \end{bmatrix}. \quad (21)$$

Importantly, because the parameters for each output are exactly the same on both single support and double support domain, the corresponding controller can easily be implemented on the real robot. In particular, the controllers for the affine control system with relative degree two outputs are defined specifically for each domain:

$$u_v^{(\alpha,\varepsilon)}(\theta_e,\dot\theta_e) =$$

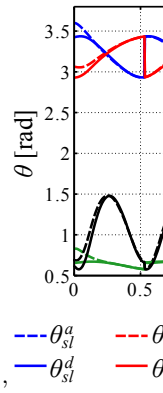

$$-\mathcal{A}_v^{-1}(\theta_e,\dot\theta_e)\left(L_{f_v}^2 y(\theta_e,\dot\theta_e) + 2\varepsilon L_{f_v} y(\theta_e,\dot\theta_e) + \varepsilon^2 y(\theta_e)\right),$$

Outputs tracking started from a perturbed point

with $\mathcal{A}_v(\theta_e,\dot\theta_e) = L_{g_v}L_{f_v}y(\theta_e,\dot\theta_e)$ the decoupling matrix for $v \in \{\mathbf{ss},\mathbf{ds}\}$. Again, the choice of outputs implies that this matrix is nonsingular.

Hybrid System. With these feedback controllers introduced for both phases, we obtain a hybrid system:

$$\mathscr{H}_A^{(\alpha,\varepsilon)} = (\Gamma_A, \mathcal{D}_A, S_A, \Delta_A, F_A), \quad (23)$$

where Γ_A, $\mathcal{D}_A$, S_A and Δ_A are as in (2). Also, $F_A = \{f_{\mathbf{ss}}^{(\alpha,\varepsilon)}, f_{\mathbf{ds}}^{(\alpha,\varepsilon)}\}$ is the set of feedback vector fields where:

$$f_{\mathbf{ss}}^{(\alpha,\varepsilon)}(\theta_e,\dot\theta_e) = f_{\mathbf{ss}}(\theta_e,\dot\theta_e) + g_{\mathbf{ss}}(\theta_e,\dot\theta_e)u_{\mathbf{ss}}^{(\alpha,\varepsilon)}(\theta_e,\dot\theta_e), \quad (24)$$

$$f_{\mathbf{ds}}^{(\alpha,\varepsilon)}(\theta_e,\dot\theta_e) = f_{\mathbf{ds}}(\theta_e,\dot\theta_e) + g_{\mathbf{ds}}(\theta_e,\dot\theta_e)u_{\mathbf{ds}}^{(\alpha,\varepsilon)}(\theta_e,\dot\theta_e). \quad (25)$$

Clearly, each individual vector field depends on ε and the parameters for their respective domains, α. The goal of SLIP inspired optimization is to design the parameters α such that the hybrid system $\mathscr{H}_{(\alpha,\varepsilon)}$ has a stable periodic orbit, i.e., a stable walking gait, for sufficiently large ε.

Zero Dynamics. The goal of the feedback control law in (22) is to drive the outputs $y(\theta_e) \to 0$ exponentially. In other words, the controller drives the system dynamics to a parameterized smooth surface, termed as the *zero dynamics surface* [3], with exponential stability. Now we will define them specifically for each domain. First, we consider the *single support* domain; when we consider the generalized coordinates θ_e, the *zero dynamics surface* is defined as:

$$\mathbf{Z}_{\mathbf{ss},\alpha} = \{(\theta_e,\dot\theta_e) \in \mathcal{D}_{\mathbf{ss}} : y(\theta_e) = \mathbf{0}, L_{f_{\mathbf{ss}}}y(\theta_e,\dot\theta_e) = \mathbf{0}\}, \quad (26)$$

where $\mathbf{0}$ is a vector of zeros. Note that we make the dependence of the *zero dynamics surface* on the set of domains explicit. Similarly, for the *double support* domain, we have:

$$\mathbf{Z}_{\mathbf{ds},\alpha} = \{(\theta_e,\dot\theta_e) \in \mathcal{D}_{\mathbf{ds}} : y(\theta_e) = \mathbf{0}, L_{f_{\mathbf{ds}}}y(\theta_e,\dot\theta_e) = \mathbf{0}\}. \quad (27)$$

With the invertible decoupling matrix due to the proper choice of the outputs, the feedback control law in (22) restricts the dynamics to the *zero dynamics surface*. Pick

$\theta_z = \{p_x, p_z, \theta_T, \theta_b\}$ with

$$\theta_z = [\mathbf{I}_{7\times 7} \quad \mathbf{0}_{7\times 4}]\,\theta_e := H_z\theta_e. \tag{28}$$

Define $x_z := (\theta_z, \dot{\theta}_z) \in \mathbf{Z}_{v,\alpha}$, the unactuated states in the Lagrangian model (10), wherein θ_z constitutes a set of local coordinates for $\mathbf{Z}_{v,\alpha}$, where $v \in \{\mathbf{ss}, \mathbf{ds}\}$. In particular, we can write the equation of the zero dynamics for a given domain $\mathcal{D}_v$ as

$$\dot{x}_z = q_v(x_z, \alpha) \tag{29}$$

for a proper selection of outputs and parametrized time defined in Sect. 3, and ground reaction forces computed from the state variables. That being said, the zero dynamics surface only depends on the parameter set of the feedback control law. In fact, we can reconstruct actuated states of the system in the terms of $(\theta_z, \dot{\theta}_z)$ and parameters α when it is on the *zero dynamics surface*.

With this notation in mind, we can now derive the equation of zero dynamics, independent of the control input. First, we consider the case of *single support* domain. From the continuous dynamics equation (10), we can write the unactuated component as,

$$D(\theta_z)\ddot{\theta}_z + H(\theta_z, \dot{\theta}_z) + \kappa_z(\theta_e, \dot{\theta}_e) = J_{es}(\theta_z)^T F_s, \tag{30}$$

where, $\kappa_z(\theta_e, \dot{\theta}_e)$ is the upper 7 rows of the κ in (11). It will be seen from (42) and (43) that, $(\theta_m, \dot{\theta}_m)$ in the expression of κ are a function of parameter α and linearized hip position, which actually only depends on the robots unactuated states. Therefore, we can write that,

$$\kappa_z(\theta_e, \dot{\theta}_e) = \kappa_z(\theta_z, \dot{\theta}_z, \alpha).$$

To fully determine the zero dynamics, the holomonic constraints are differentiated twice and set equal to zero:

$$\frac{\partial J_{es}(\theta_z)\dot{\theta}_z}{\partial t} = J_{es}(\theta_z)\ddot{\theta}_z + \dot{J}_{es}(\theta_z, \dot{\theta}_z)\dot{\theta}_z = 0. \tag{31}$$

Solving (30) and (31) simultaneously for F_s yields,

$$F_s(\theta_z, \dot{\theta}_z) = (J_{es}(\theta_z)D(\theta_z)^{-1}J_{es}(\theta_z)^T)^{-1}(-\dot{J}_{es}(\theta_z, \dot{\theta}_z)\dot{\theta}_z + J_{es}(\theta_z)D(\theta_z)^{-1}(H(\theta_z, \dot{\theta}_z) + \kappa_z(\theta_z, \dot{\theta}_z.\alpha))) \tag{32}$$

By substituting (32) into (30), we have the zero dynamics equation of *single support* domain in the form of (29) with,

$$q_{\mathbf{ss}}(x_z, \alpha) = \begin{bmatrix} \dot{\theta}_z \\ D^{-1}(-\kappa - H + J_{es}^T F_s) \end{bmatrix}. \tag{33}$$

Similarly for the *double support* domain, the following equation holds,

$$q_{\mathbf{ds}}(x_z, \alpha) = \begin{bmatrix} \dot{\theta}_z \\ D^{-1}(-\kappa - H + J_{es}^T F_s + J_{ens}^T F_{ns}) \end{bmatrix}. \tag{34}$$

where $[F_s \quad F_{ns}]^T$ can be obtained analogously from (32) by replacing J_{es} by $[J_{es} \quad J_{ens}]$.

Main observation. The advantage of zero dynamics is that, instead of full-order dynamics, the low dimensional zero dynamics can be used in the optimization problem introduced in next section *if* the zero dynamics are invariant through the impacts of the system. In particular, the hybrid system $\mathscr{H}_A^{(\alpha,\varepsilon)}$ in (23) obtained by applying human-inspired control to the hybrid control system $\mathscr{HC}_A$ in (2) has *hybrid zero dynamics* if:

$$\Delta_{\mathbf{ss}\to\mathbf{ds}}(S_{\mathbf{ss}\to\mathbf{ds}} \cap \mathbf{Z}_{\mathbf{ss},\alpha}) \subset \mathbf{Z}_{\mathbf{ds},\alpha}, \tag{HZD1}$$

$$\Delta_{\mathbf{ds}\to\mathbf{ss}}(S_{\mathbf{ds}\to\mathbf{ss}} \cap \mathbf{Z}_{\mathbf{ds},\alpha}) \subset \mathbf{Z}_{\mathbf{ss},\alpha}. \tag{HZD2}$$

The result of hybrid zero dynamics is a stable periodic multi-domain walking gait for the full order system given a stable limit cycle in the (hybrid) zero dynamics. This can be formally summarized as follows:

Theorem 1. *If the hybrid system $\mathscr{H}_A^{(\alpha,\varepsilon)}$ in* (23) *satisfies* (HZD1) *and if $\mathcal{O}_Z \subset \mathbf{Z}_{\mathbf{ds}} \cup \mathbf{Z}_{\mathbf{ss}}$ is an exponentially stable periodic orbit for the zero dynamics in* (29)*, then there exists $\varepsilon > 0$, such that $\mathcal{O} = \iota_0(\mathcal{O}_Z)$ is an exponentially stable periodic orbit of the full order system, where $\iota_0 : \mathbf{Z}_{\mathbf{ds}} \cup \mathbf{Z}_{\mathbf{ss}} \to \mathcal{D}_{\mathbf{ss}} \cup \mathcal{D}_{\mathbf{ds}}$ is the canonical embedding.*

Space constraints do not allow for a proof of this result, but it essentially follows in a straightforward manner from the results of [5] coupled with the fact that $\Delta_{\mathbf{ds}\to\mathbf{ss}} = \mathbf{I}$. This is why only (HZD1) is required and why, in the future, this condition will be denoted by simply (HZD).

4. OPTIMIZATION

In this section, we will discuss the process of obtaining control parameters and an initial condition on the zero dynamics that result in *hybrid zero dynamics* (HZD) while producing outputs that are as close as possible to those of the SLIP model. More formally, an optimization problem is constructed to solve for parameters of the human-inspired controller α, and a fixed point $(\theta_z^-, \dot{\theta}_z^-)$ that guarantees HZD while simultaneously generating a stable walking gait.

SLIP Inspired Optimization. This section utilizes the fact that the *zero dynamic surfaces* in (26) and (27) are invariant under the flow of closed-loop continuous dynamics, while it is not necessarily invariant for the discrete dynamics. In particular, the invariance of the zero dynamics will be disturbed at the discrete impacts that occur as a result of contact points changing. For the hybrid system of (2), the only impact occurs when the robot transitions from the *single support* domain to the *double support* domain. The goal of this paper is to find a parameter set α^*, which guarantees hybrid invariance of the hybrid system of (2) while tracking the center of mass (CoM) trajectory of the SLIP model as close as possible. In particular, we construct the following constrained optimization problem, called *SLIP Inspired Optimization*:

$$\alpha^* = \underset{\alpha\in\mathbb{R}^{4\times 5}}{\operatorname{argmin}} \ \mathrm{Cost}_{\mathrm{SLIP}}(\alpha) \tag{35}$$

$$\text{s.t} \quad \Delta_{\mathbf{ss}\to\mathbf{ds}}(S_{\mathbf{ss}\to\mathbf{ds}} \cap \mathbf{Z}_{\mathbf{ss},\alpha}) \subset \mathbf{Z}_{\mathbf{ds},\alpha}, \tag{HZD}$$

with the SLIP-model-based cost function defined as:

$$\mathrm{Cost}_{\mathrm{SLIP}}(\alpha) = \sum_{k=1}^{K} \sum_{i\in\{x,z\}} \left(p_{com,i}^S[k] - p_{com,i}\left(y^H(t^S[k], \alpha)\right)\right)^2, \tag{36}$$

where discrete times, $t^S[k]$, and discrete values of the CoM position for the SLIP gait, $p_{com,i}^S[k]$, for $i \in \{x, z\}$ obtained from the SLIP walking gait found in Fig. 3, and $p_{com}\left(y^H(t^S[k], \alpha)\right)$ is the approximate center of mass position of the robot computed from the outputs characterized

by the canonical walking function. The end result is the least square fit of the CoM trajectory of the robot to that of SLIP model. In other words, we seek to "shape" the dynamics of the robot as close to SLIP model dynamics as possible. The formal goal of this section is to reframe the constraints of (HZD) in a way that it can be practically solvable.

Hybrid Zero Dynamics As discussed in previous section, a hybrid system has *hybrid zero dynamics* (HZD) if the zero dynamics are invariant through the impact. For a rigid body system, the pre-impact states can be explicitly solved for in terms of the parameter α [2]. However, because the system being considered has series elastic actuators, it is not possible to solve explicitly due to high dimensions of zero dynamics surface of the system. The difficulty comes from the fact that the pre-impact states of the zero dynamics coordinates $(\theta_z^-, \dot{\theta}_z^-) \in S_{\mathbf{ss}\to\mathbf{ds}} \cap \mathbf{Z}_{\mathbf{ss},\alpha}$ need to be solved by integrating the dynamics defined in (29).

We assume that a set of points $(\theta_z^-, \dot{\theta}_z^-)$ are the local coordinates of the zero dynamics on the guard. Due to the fact that the guard function $h_{ns}(\theta_e)$ only depends on the rigid body configurations, which is the same as $h_{ns}(\theta_z)$ in this case, the following constraints need to be satisfied:

$$h_{ns}(\theta_z^-, \dot{\theta}_z^-) = 0, \tag{C1}$$

$$dh_{ns}(\theta_z^-)\dot{\theta}_z^- < 0. \tag{C2}$$

Now we expand our parameter set by defining,

$$\beta := \{\alpha, \theta_z^-, \dot{\theta}_z^-\}.$$

The advantage of this definition is that we can solve the pre-impact states explicitly in the terms of β, and simplify the constraints to the same form as in [2]. A point $(\vartheta(\beta), \dot{\vartheta}(\beta)) \in S_{\mathbf{ss}\to\mathbf{ds}} \cap \mathbf{Z}_{\mathbf{ss},\alpha}$ that depends on these parameters can be obtained by solving the equations:

$$\vartheta(\beta) := \theta_e \quad \text{s.t.} \quad y(\mathcal{R}\Delta_{\theta_e}\theta_e) = \mathbf{0}_4 \tag{37}$$

$$\dot{\vartheta}(\beta) = Y^{-1}(\vartheta(\beta)) \begin{bmatrix} \dot{\theta}_z^- \\ \mathbf{0}_4 \end{bmatrix}, \tag{38}$$

where $\mathcal{R}$ is the relabeling matrix and,

$$Y(\vartheta(\beta)) = \begin{bmatrix} H_z \\ dy(\vartheta(\beta)) \end{bmatrix}$$

where H_z is defined in (28) such that $\theta_z = H_z\theta_e$. The equation (37) is easy to solve by the fact that $\theta_e^+ = \mathcal{R}\Delta_{\theta_e}\theta_e$ and $\tau(\mathcal{R}\Delta_{\theta_e}\theta_e) = 0$ implying that: $y(\theta_e^+) = y^a(\theta_e^+) - y^d(0)$. With the proper choice of the outputs, the matrix $Y(\vartheta(\beta))$ is invertible. Thus the (HZD) of the system can be stated as,

$$y(\vartheta(\beta)) = \mathbf{0}, \tag{C3}$$

$$dy\left(\mathcal{R}\Delta_{\theta_e}\vartheta(\beta)\right)\mathcal{R}\Delta_{\dot{\theta}_e}(\vartheta(\beta))\dot{\vartheta}(\beta) = \mathbf{0}, \tag{C4}$$

which guarantee the hybrid invariance of the system through impacts [2].

Physical Constraints. To achieve a physically permissible walking gait, several constraints are imposed on the optimization. The computations of the physical constraints are performed by integrating the zero dynamics of (29) over both *double support* and *single support* domains with the initial condition $\Delta_{\mathbf{ss}\to\mathbf{ds}}(\vartheta(\beta), \dot{\vartheta}(\beta))$. Those constraints are shown as follows:

Ground Reaction Forces: For the *double support* domain, the normal ground reaction forces on non-stance foot should be positive to prevent the reaction force from "pulling" the robot against the ground, i.e.,

$$F_{ns}^z(\theta_z, \dot{\theta}_z, \alpha) > 0, \quad (\theta_z, \dot{\theta}_z) \in \mathcal{D}_{\mathbf{ds}}. \tag{C5}$$

For the *single support* domain, the normal ground reaction forces on stance foot should be positive, otherwise the robot will leave the ground and enter the flight phase, which is not in the scope of this paper. Therefore, we require that:

$$F_s^z(\theta_z, \dot{\theta}_z, \alpha) > 0, \quad (\theta_z, \dot{\theta}_z) \in \mathcal{D}_{\mathbf{ss}}. \tag{C6}$$

The ground reaction forces can be computed by (32).

Friction: To prevent the stance foot from sliding, the following constraint is imposed:

$$F_s^x(\theta_z, \dot{\theta}_z, \alpha) < \mu F_s^z(\theta_z, \dot{\theta}_z, \alpha), \tag{C7}$$

where μ is the coefficient of static friction for the contact between stance foot and the ground.

Foot Clearance: From the definition of the $\mathcal{D}_{\mathbf{ss}}$, the height of the non-stance foot needs to be above the ground during the *single support* domain. The constraint can be expressed as

$$h_{ns}(\theta_z) > 0, \quad (\theta_z, \dot{\theta}_z) \in \mathcal{D}_{\mathbf{ss}}. \tag{C8}$$

Touch Down Angle: To achieve stable walking with the ideal SLIP model discussed in Fig. 3, it requires that the touch down angle, or the angle of attack, denoted as θ_t, needs to be a certain value, $\theta_{\mathcal{TD}}$, determined from the optimal SLIP gait. With the goal of matching the SLIP model dynamics as close as possible, we impose a constraint that the touch down angle of the robot, which is a function of post impact state $\vartheta(\beta)$ in (37), equals the desired value of the stable SLIP walking gait:

$$\theta_t(\vartheta(\beta)) = \theta_{\mathcal{TD}}. \tag{C9}$$

We now have the necessary framework in which to restate the *SLIP Inspired Optimization* problem for multi-domain walking:

$$\beta^* = \underset{\beta\in\mathbb{R}^{4\times5}\times T\mathcal{Q}_z}{\operatorname{argmin}} \ \text{Cost}_{\text{SLIP}}(\beta) \tag{39}$$

$$\text{s.t} \quad \text{(C1)} - \text{(C9)}. \tag{C}$$

where $\mathcal{Q}_z \subset \mathcal{Q}$ is the configuration space of the zero dynamics coordinates θ_z. The end result is a stable multi-domain walking gait with $\beta = (\alpha, \theta_z^-, \dot{\theta}_z^-)$ consists of the parameters of the human walking function α, and the pre-impact states $(\theta_z^-, \dot{\theta}_z^-)$ of the zero dynamics. The stability of the gait is validated numerically through the use of the *Poincaré* map only for the zero dynamics.

Taking $S_{\mathbf{ss}\to\mathbf{ds}}$ as the *Poincaré* section, define the *Poincaré* map $P^\varepsilon : S_{\mathbf{ss}\to\mathbf{ds}} \to S_{\mathbf{ss}\to\mathbf{ds}}$ which is a partial function:

$$P^\varepsilon(\theta_z, \dot{\theta}_z) = \phi^{\mathbf{ss}}_{T_{\mathbf{ss}}(\theta_z,\dot{\theta}_z)}(\Delta_{\mathbf{ss}\to\mathbf{ss}}(\theta_z^-, \dot{\theta}_z^-)), \tag{40}$$

with $\Delta_{\mathbf{ss}\to\mathbf{ss}}(\theta_z^-, \dot{\theta}_z^-)$ defined as,

$$\Delta_{\mathbf{ss}\to\mathbf{ss}}(\theta_z^-, \dot{\theta}_z^-) = \Delta_{\mathbf{ds}\to\mathbf{ss}}(\phi^{\mathbf{ds}}_{T_{\mathbf{ds}}(\theta_z,\dot{\theta}_z)}(\Delta_{\mathbf{ss}\to\mathbf{ds}}(\theta_z^-, \dot{\theta}_z^-)))$$

where, for $v \in \{\mathbf{ss}, \mathbf{ds}\}$, ϕ^v is the flow generated by the zero dynamics vector field $q_v^{(\alpha,\varepsilon)}$ and $T_v(\theta_z, \dot{\theta}_z)$ is the *time-to-impact* function determined by the first time the flow intersects with the corresponding guard, respectively.

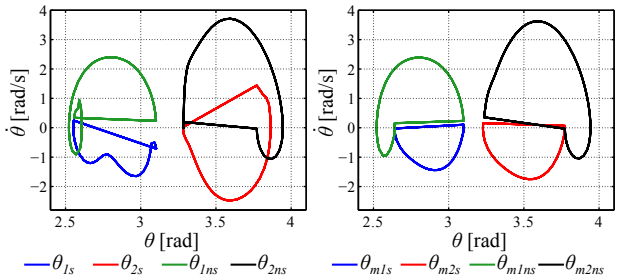

(a) Joint Angles (b) Motor Angles

Figure 5: Stable periodic orbits in the joint angles and motor angles for the walking gait generated through the SLIP-inspired optimization. Note that the difference in shape between (a) and (b) demonstrate the compliance present in the robotic system being considered.

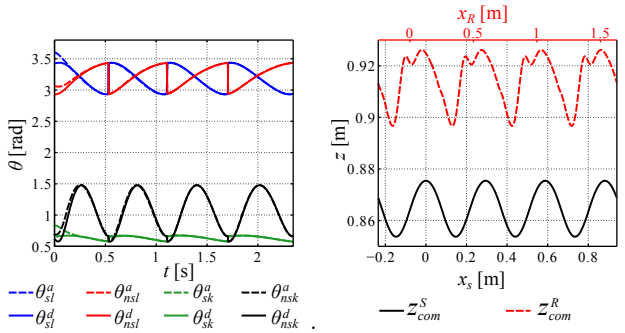

(a) Outputs (b) Center of Mass Position

Figure 6: Simulation results: (a) Desired versus actual outputs starting from a perturbed point. (b) A comparison of the center of mass trajectory between the ideal SLIP gait and the full-order robotic model.

The point $(\theta_z^-, \dot{\theta}_z^-)$ on $S_{\mathbf{ss}\to\mathbf{ds}}$ is a fixed point of P^ε if and only if $(\theta_z^-, \dot{\theta}_z^-) = P^\varepsilon(\theta_z^-, \dot{\theta}_z^-)$. Moreover, if P^ε is exponentially stable with a sufficiently large gain ε, then the fixed point is a stable fixed point and the equivalence of the stability of the fixed point and the corresponding periodic orbit implies that the zero dynamics of the system has a stable periodic orbit [22]. Therefore, by applying the result of Theorem 1 in this paper, we can conclude that parameters obtained from the optimization result in a periodic orbit on the full order system, and thus a stable walking gait is achieved.

5. IMPLEMENTATION AND RESULTS

This section discusses the simulated and experimental results on ATRIAS for the multi-domain walking gait previously obtained. The simulation results show the control system's stability, convergence after perturbations, and SLIP-like behavior. Experimental results show sustainable and dynamic walking on a real robotic platform [1].

Simulation Results. A walking gait was generated through the SLIP-inspired optimization (39), subject to constraints that ensure a physically realizable gait on hardware. The gait was then simulated using the human-inspired controllers introduced in Sect. 3. The resulting periodic orbits can be seen in Fig. 5. The robustness of the gait was also investigated; the system was simulated from a perturbed initial condition to show the output tracking convergence, as depicted in Fig. 6a. Finally, the stability of the gait was numerically verified. For $\varepsilon = 100$, the maximum magnitude of the *Poincaré* eigenvalues, 0.7135, is less than one, establishing the stability of the gait.

Due to the SLIP-inspired nature of the optimization, the full-order model gait behavior was compared to the ideal SLIP model gait. Although they have different speeds and step lengths, simulation shows that the planar center of mass trajectory of the full-order gait exhibits patterns very similar to that of the SLIP gait, as illustrated in Fig. 6b. Note that the x positions of the two trajectories are on different scales. To show the similarities, x-axis scaling was adjusted between the two gaits so that they are in phase. This difference could be a result of the ideal SLIP model's massless leg assumption. In the SLIP model, the leg is assumed massless, enabling instantaneous swing leg movements during single support phase. Even though the ATRIAS legs are designed to be near massless, the motors have large reflected inertias resulting in physical limitations on the leg swing. Therefore, SLIP gaits with very short single support phases may not be physically possible with the full-order model. An additional selection criteria could be used to overcome this, selecting SLIP gaits with an adequate single support duration to allow for leg swing. Moreover, to achieve sustainable walking on a real robot, a proper foot clearance constraint is needed with a maximum non-stance foot height. To satisfy this constraint, the optimization will tend to find gaits with a comparatively high center of mass position. Despite these differences, the full-order system's walking gait is remarkably SLIP-like.

Controller Implementation. For practical realization, we want to find the desired robot joint angles and velocities at each iteration through inverse projection from the HZD surface. Given the HZD surface, we define

$$\begin{aligned} \xi_1 &= \delta p_{\text{hip}}(\theta_e) := c_1\theta_e + c_0, \\ \xi_2 &= \delta \dot{p}_{\text{hip}}(\theta_e) := c_1\dot{\theta}_e, \end{aligned} \tag{41}$$

where $c_1 \in \mathbb{R}^{11\times 1}$, $c_0 \in \mathbb{R}$ are obtained from (19). Since ξ_1 is the linearized position of the hip used to parameterize time (18), we can write $y^d(\tau(\theta_e), \alpha) = y^d(\xi_1, \alpha)$.

Moreover, as a result of selecting outputs that are linear functions of motor angles θ_m, the actual outputs can be written as $y^a(\theta_e) = \mathcal{H}\theta_m$ for $\mathcal{H} \in \mathbb{R}^{4\times 4}$ with full row rank. Thus, when the system is constrained to the zero dynamics surface via feedback control, the actual outputs are equal to the desired outputs. Therefore, defining the following functions

$$\Psi(\xi_1, \alpha) := \mathcal{H}^{-1} y^d(\xi_1, \alpha), \tag{42}$$

$$\Phi(\xi_1, \alpha) := \mathcal{H}^{-1} \frac{\partial y^d(\xi_1, \alpha)}{\partial \xi_1} \tag{43}$$

yields the desired motor angles and their corresponding velocities, $\theta_m^d = \Psi(\xi_1, \alpha)$ and $\dot{\theta}_m^d = \Phi(\xi_1, \alpha)\xi_2$. That is, we can reconstruct the desired motor angles and velocities from the system outputs on the HZD surface. Tracking these joint angles and velocities on the robot is equivalent to tracking the outputs of the robot, i.e., the restriction of the dynamics to the partial zero dynamics surface is maintained.

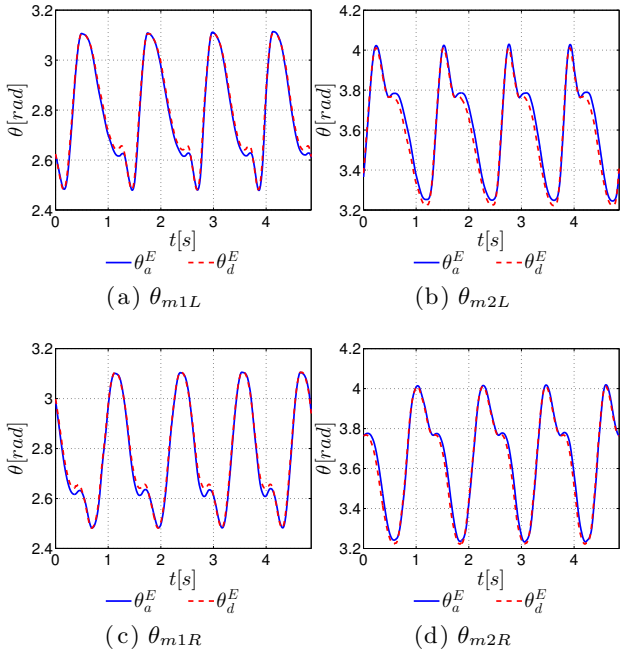

(a) θ_{m1L} (b) θ_{m2L}

(c) θ_{m1R} (d) θ_{m2R}

Figure 7: Comparison of the actual θ_a^E vs. desired θ_d^E motor angle trajectories from the experimentation.

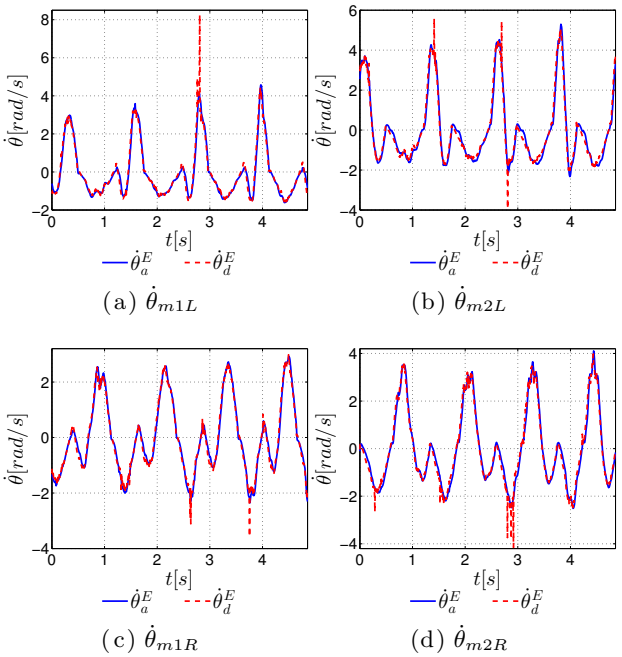

(a) $\dot{\theta}_{m1L}$ (b) $\dot{\theta}_{m2L}$

(c) $\dot{\theta}_{m1R}$ (d) $\dot{\theta}_{m2R}$

Figure 8: Comparison of actual $\dot{\theta}_a^E$ vs. desired $\dot{\theta}_d^E$ motor velocities trajectories from experimentation.

PD controllers are then used to track the desired motor angles and velocities obtained from the HZD reconstruction:

$$\tau_{PD} = -K_p(\theta_m^a - \theta_m^d) - K_d(\dot{\theta}_m^a - \dot{\theta}_m^d), \qquad (44)$$

where K_p and K_d are proportional and derivative constant matrices, respectively. Here, the elements of the K_p and K_d matrices depend on their corresponding motors.

Experimental Setup. ATRIAS is supported by a boom that constrains it to the sagittal plane so as to emulate a 2D planar robot. In addition, boom encoders at each degree of freedom provide full feedback on the robot's torso position and rotation relative to the world. During experiments the boom also functions as a safety mechanism to catch the robot in the event of a fall; it does not provide any support in the sagittal plane at any other time.

Each experiment was conducted in a similar manner. The control system was initially enabled while ATRIAS was suspended in the air, allowing the software to drive the robot to an initial pose. ATRIAS was then lowered to the ground and manually given an initial impulse to initiate the walking motion. Fig. 7 and Fig. 8 show the tracking of the motor angles and velocities of the left and right legs during four walking steps with the left leg as the stance leg for the first step. Note that the subscripts 'L' and 'R' in the subtitles represent the left and right leg, respectively. The tracking errors are exceptionally small with motor torque inputs that remain within the robots capabilities (see Fig. 10). This results in a dynamically stable walking gait that visually appears very "SLIP-like". The snapshot in Fig. 9 illustrates the extraordinary similarities between the simulated and experimental gaits. The video of the experiment shows sustainable walking with ATRIAS and is available online [1].

Conclusions. This paper successfully demonstrates underactuated multi-domain walking on the compliant bipedal

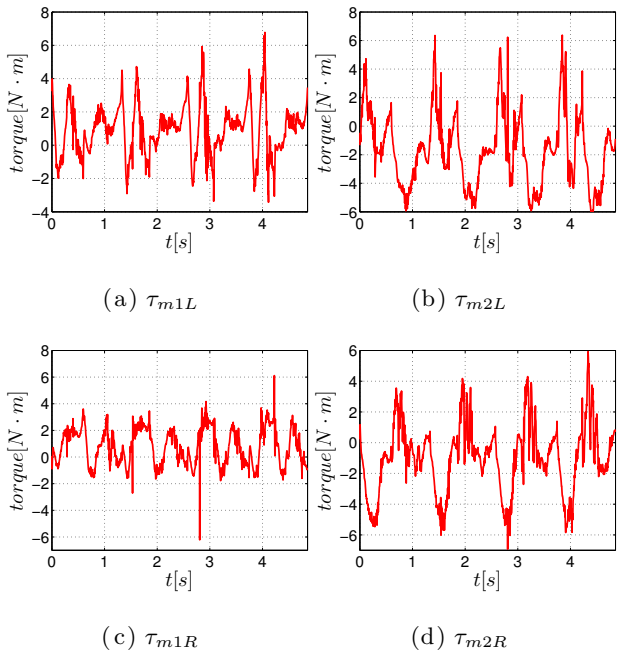

(a) τ_{m1L} (b) τ_{m2L}

(c) τ_{m1R} (d) τ_{m2R}

Figure 10: Corresponding torque input of each motors.

robot ATRIAS. Our approach starts with a passive walking gait generated by a reduced-order SLIP model that captures the primary dynamics of the robot. From this an optimal walking controller is derived using hybrid zero dynamics. Comparisons of the simulated and experimental results illustrate the effectiveness of the proposed methods and highlight the remarkably natural look of the gait.

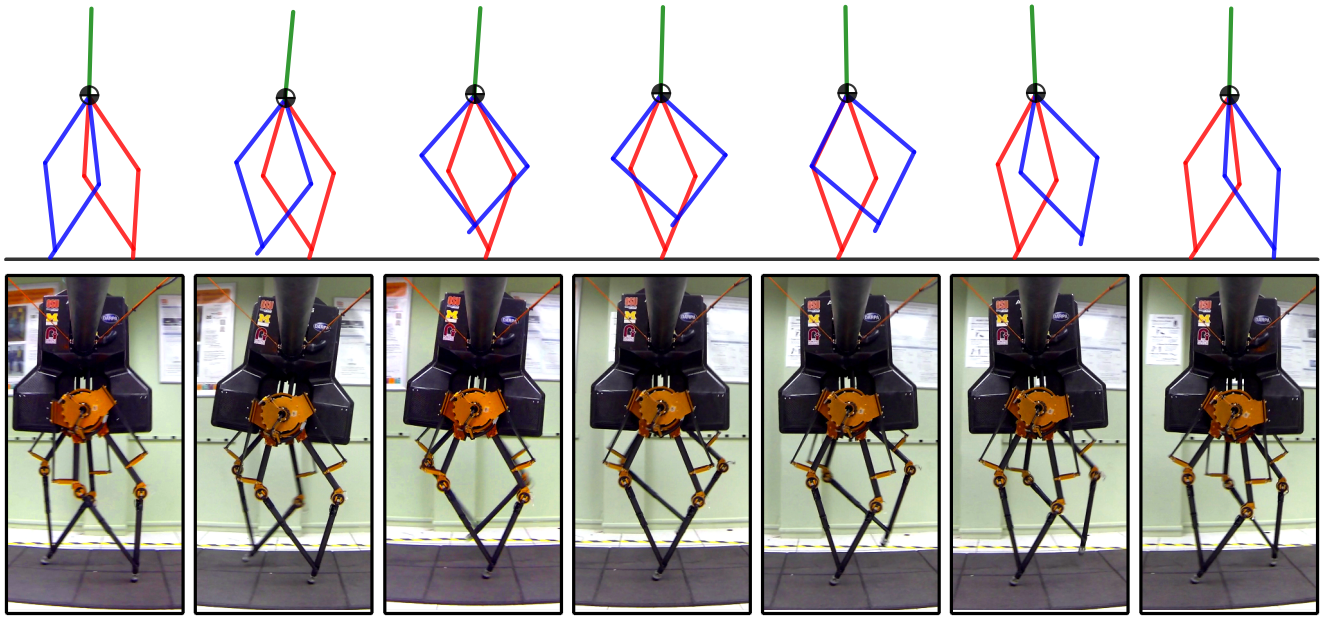

Figure 9: The walking gait snapshot comparison of the simulation and experimental results with ATRIAS over one step.

6. REFERENCES

[1] Sustained walking of ATRIAS 2.1: http://youtu.be/yiEbWwC-sR0.

[2] A. D. Ames. First steps toward automatically generating bipedal robotic walking from human data. In *Robotic Motion and Control 2011*, volume 422 of *LNICS*, pages 89–116. Springer, 2012.

[3] A. D. Ames. First steps toward underactuated human-inspired bipedal robotic walking. In *Robotics and Automation (ICRA), 2012 IEEE International Conference on*, pages 1011–1017. IEEE, 2012.

[4] A. D. Ames, E. A. Cousineau, and M. J. Powell. Dynamically stable bipedal robotic walking with NAO via human-inspired hybrid zero dynamics. In *Hybrid Systems: Computation and Control*, pages 135–44, Beijing, Apr. 2012.

[5] A. D. Ames, K. Galloway, J. Grizzle, and K. Sreenath. Rapidly exponentially stabilizing control lyapunov functions and hybrid zero dynamics. *To appear in IEEE Trans. Automatic Control*, 2013.

[6] A. D. Ames, R. Vasudevan, and R. Bajcsy. Human-data based cost of bipedal robotic walking. In *14th Intl. Conf. on Hybrid Systems: Computation and Control*, pages 153–62, Chicago, Apr. 2011.

[7] G. A. Bekey. *Autonomous robots: from biological inspiration to implementation and control*. MIT Press, May 2005.

[8] R. Blickhan. The spring-mass model for running and hopping. *Journal of biomechanics*, 22(11), 1989.

[9] R. Blickhan and R. Full. Similarity in multilegged locomotion: bouncing like a monopode. *Journal of Comparative Physiology A*, 173(5):509–517, 1993.

[10] D. J. Braun and M. Goldfarb. A control approach for actuated dynamic walking in bipedal robots. *IEEE Trans. on Robotics*, 25(6):1292–1303, Dec. 2009.

[11] G. A. Cavagna, N. C. Heglund, and C. R. Taylor. Mechanical work in terrestrial locomotion: two basic mechanisms for minimizing energy expenditure. *American Journal of Physiology-Regulatory, Integrative and Comparative Physiology*, 233(5):R243–R261, 1977.

[12] R. Full and D. Koditschek. Templates and anchors: Neuromechanical hypotheses of legged locomotion on land. *The Journal of Experimental Biology*, 202:3325–3332, 1999.

[13] J. W. Grizzle, C. Chevallereau, A. D. Ames, and R. W. Sinnet. 3D bipedal robotic walking: models, feedback control, and open problems. In *IFAC Symposium on Nonlinear Control Systems*, Bologna, Sept. 2010.

[14] C. Hubicki, J. Grimes, M. Jones, D. Renjewski, A. Spröwitz, A. Abate, and J. Hurst. ATRIAS: Enabling agile biped locomotion with a template-driven approach to robot design. *Submitted to International Journal of Robotics Research*, 2014.

[15] Y. Hürmüzlü and D. B. Marghitu. Rigid body collions of planar kinematic chains with multiple contact points. *Intl. J. of Robotics Research*, 13(1):82–92, 1994.

[16] A. D. Kuo, J. M. Donelan, and A. Ruina. Energetic consequences of walking like an inverted pendulum: step-to-step transitions. *Exercise and sport sciences reviews*, 33(2):88–97, 2005.

[17] T. McGeer. Passive dynamic walking. *the international journal of robotics research*, 9(2):62–82, 1990.

[18] B. Morris and J. Grizzle. Hybrid invariance in bipedal robots with series compliant actuators. In *Decision and Control, 2006 45th IEEE Conference on*, pages 4793–4800. IEEE, 2006.

[19] A. Ramezani, J. W. Hurst, K. A. Hamed, and J. Grizzle. Performance analysis and feedback control of ATRIAS, a 3D bipedal robot. *accepted ASME J. Dynamic Systems Measurement and Control*, 2012.

[20] M. Srinivasan. Fifteen observations on the structure of energy-minimizing gaits in many simple biped models. *Journal of The Royal Society Interface*, 8(54):74–98, 2011.

[21] M. Srinivasan and A. Ruina. Computer optimization of a minimal biped model discovers walking and running. *Nature*, 439(7072):72–75, 2005.

[22] E. R. Westervelt, J. W. Grizzle, C. Chevallereau, J. H. Choi, and B. Morris. *Feedback Control of Dynamic Bipedal Robot Locomotion*. CRC Press, Boca Raton, 2007.

[23] E. R. Westervelt, J. W. Grizzle, and D. E. Koditschek. Hybrid zero dynamics of planar biped walkers. *IEEE Trans. on Automatic Control*, 48(1):42–56, 2003.

[24] S. N. Yadukumar, M. Pasupuleti, and A. D. Ames. From formal methods to algorithmic implementation of human inspired control on bipedal robots. In *Algorithmic Foundations of Robotics X*, pages 511–526. Springer, 2013.